Geo-Mar Lett (2014) 34:199–213
DOI 10.1007/s00367-014-0357-3

ORIGINAL

How to evacuate 10 km^3 of mud: saturate with gas and decrease the pressure!

Patrice Imbert · Bernard Geiss · Núria Fatjó de Martín

Received: 17 June 2013 / Accepted: 22 January 2014 / Published online: 26 February 2014

Abstract The crest of the Absheron anticline in the South Caspian Basin at a few hundred meters below the present seafloor shows a subcircular depression about 8 km in diameter and 200 m deep, bounded by steep edges dipping 15° to 45° into it. The depression and the surrounding series are respectively filled and overlain by a regional mass-transport deposit (MTD) 150 m thick outside the depression and 300 m thick inside, composed mostly of extensional blocks. Geometric and stratigraphic analyses indicate that 150 m of initially deposited sediment were removed from a closed area after burial. Seismic evidence of shallow gas accumulations below the crater-like feature suggests that gas likely played a significant role in its development. The model proposed for the emplacement of the crater is that the gas-bearing cover of a shallow gas reservoir underwent exsolution when its overburden thinned during an episode of extensional slope failure. This resulted in loss of resistance to shear and evacuation of the gas-bearing sediment, likely at the shearing base of the failed mass. This evacuation feature is considered an example where the presence of gas locally governs the morphology of an MTD. The interpreted process shows a positive feedback between slope failure and loss of strength at the base of the resulting MTD.

Responsible guest editor: C. Pierre

P. Imbert (✉)
Total CSTJF, avenue Larribau, 64000 Pau, France
e-mail: patrice.imbert@total.com

B. Geiss
Total E&P Azerbaijan, 69 Nizami Street, Baku, Azerbaijan

N. Fatjó de Martín
Cepsa E&P, Madrid, Spain

Introduction

Kilometer-scale sediment evacuation under cover is a process that has been described in several contexts—for instance, chambers of mud volcanoes (e.g., Planke et al. 2003; Stewart and Davies 2006; Deville 2009; Deville et al. 2010), silica ooze "diapirism" (e.g., Riis et al. 2005; Lawrence and Cartwright 2010), or hydrate pockmarks and collapsed pockmarks, their fossil counterpart (e.g., Sultan et al. 2010; Imbert and Ho 2012). Sediment evacuation is usually observed through the collapse/foundering of a package of sediment below its initial locus of deposition, thereby occupying the space of series that are displaced or removed during the process. In the case documented by Riis et al. (2005) and Lawrence and Cartwright (2010), biostratigraphic data from boreholes provided evidence of the stratigraphic inversion between the evacuated mass and the deposits through which evacuation had occurred. When no direct calibration (e.g., borehole) is available, diagnosis of evacuation requires evidence that the present-day position of the package interpreted as "foundered" is incompatible with normal sedimentary processes, such as erosion followed by infill, or en masse resedimentation (e.g., head scarp of a slump).

This article explores genetic relationships between large-scale mass failure and sediment remobilization in a deep-water setting off Baku in the South Caspian Basin, Azerbaijan. In this prolific onshore and offshore oil and gas province, sediment remobilization has been the subject of numerous publications this last decade, in particular related to mud volcanoes (e.g., Fowler et al. 2000; Planke et al. 2003; Yusifov and Rabinowitz 2004; Evans et al. 2006) and mud volcano systems (Stewart and Davies 2006). More recently, Richardson et al. (2011) focused on mass-transport complexes. The present study investigates a massive (several kilometers in diameter), buried crater-like structure associated with a

mass-transport deposit at the crest of the Absheron anticline.

Physical setting

The study area is located off Baku at 300–700 m water depths on the upper slope of the South Caspian Basin, 50 km to the SE of the tip of the Absheron peninsula (Fig. 1a). The interval of interest lies in the shallow subsurface at 200–500 ms two-way travel time (TWT; ca. 200–500 m) below the present-day seafloor and, based on seismic stratigraphy by Abdullayev (2000) and age dating by Ali-Zadeh and Aliyeva (2004), would be of late Quaternary age.

Basin history

The South Caspian Basin is generally interpreted as a remnant of the Paratethys Ocean (Popov et al. 2004), although there are diverging interpretations with regard to the genesis of the basin and the nature of the crust below. According to Popov et al. (2004), the Paratethys was separated from the Mediterranean Tethys domain in the Oligocene, due to the surrection of the Alps, Carpathians, Dinarides, Taurus, and Alborz. Subsequent convergence between these mountain ranges and the north European craton subdivided the Paratethys into several sub-basins, leading in particular to the formation of the South Caspian depression in the Middle Miocene (~16 Ma). When the Greater Caucasus emerged, it split the former eastern Paratethys between the southern Caspian and the Black Sea domains. The formation of the Kopet Dagh range in the northern part of present-day Iran has isolated the South Caspian Basin from the world ocean since the end of the Pliocene (Jones and Simmons 1996).

Structure

The South Caspian Basin is an aseismic block (Jackson et al. 2002) surrounded by active thrust belts associated with shallow earthquakes (<30 km). However, the northern boundary of the basin is characterized by deep earthquakes (30–76 km), interpreted by Jackson et al. (2002) and Allen et al. (2002) to indicate incipient subduction of the South Caspian Basin under the Central Caspian continental domain to the north. The basement of the South Caspian Basin remains rigid (aseismic) in this process, and the convergence is accommodated by the formation of an incipient accretionary prism with numerous anticlinal folds of the sedimentary cover detached on deeper mobile shales. This prism is known as the Absheron Ridge (Allen et al. 2002, 2003; Jackson et al. 2002). A summary sketch of its formation and structure can be found in Stewart and Davies (2006, their Fig. 1). The present study area is located in the vicinity of the crest of the W–E trending Absheron anticline.

Regional stratigraphy

The South Caspian Basin has accumulated more than 8 km of sediment since the Middle Miocene, making it one of the most rapidly subsiding basins in the world. The Miocene-Pliocene series include the group of formations known as the "Productive Series", which contain oil and gas accumulations in fluvio-deltaic sediments related to the paleo-Volga and paleo-Kura rivers (see Kalani et al. 2008; Kroonenberg et al. 2012). A subsequent increase in relative sea level resulted in the deposition of a ca. 2-km-thick interval of deep-water slope shale on top of the Productive Series. This shale interval is regionally subdivided (Abdullayev 2000) into the Akchagyl Formation (the top Akchagyl is dated at 1.7 Ma), the Absheron Formation (the top Absheron is dated at 0.7 Ma), and four formations above the top Absheron (Baku, Khazar, Khvalyn, and Novocaspian). For the purpose of this study, these four formations are informally referred to as the "post-Absheron Group".

A regional sand unit, the "Q sands" (Q for "Quaternary"), is found in the lower half of the post-Absheron Group. It was initially recognized in the wells of the neighboring Shah Deniz gas field, and its presence was confirmed by drilling in the Absheron area. The regional character of this sand unit, in combination with its deep-water setting and the absence of any channelized character on seismic profiles, suggest that it consists of a turbidite lobe or lobe complex.

The base of the present study interval is the top of the Absheron Formation. The corresponding seismic marker had been identified in the neighboring Shah Deniz area by Fowler et al. (2000), based on a three-dimensional (3-D) seismic block. It was extrapolated to the Absheron 3-D block using a larger-scale, regional two-dimensional (2-D) seismic grid (see below for more information on these three datasets).

Figure 2a is a regional-scale 2-D seismic profile extending from the shelf into deeper waters in the study area. The variations of the offlap break (cf. Vail et al. 1991) with time are clearly expressed and indicate that the study area lay well beyond the depositional shoreline break, i.e., in deep water, throughout the interval of interest.

The 2-D seismic profile in Fig. 2b runs perpendicular to the profile reported in Fig. 2a, and shows four seismically chaotic packages sandwiched between intervals having a parallel-continuous character. These correspond to the initial definition of mass-transport deposits (MTDs) proposed by Weimer (1989). Reviews of MTDs imaged by better quality seismics than in that initial work can be found in Moscardelli et al. (2006) and Bull et al. (2009); a detailed study of MTDs around the Shah Deniz anticline is provided by Richardson et al.

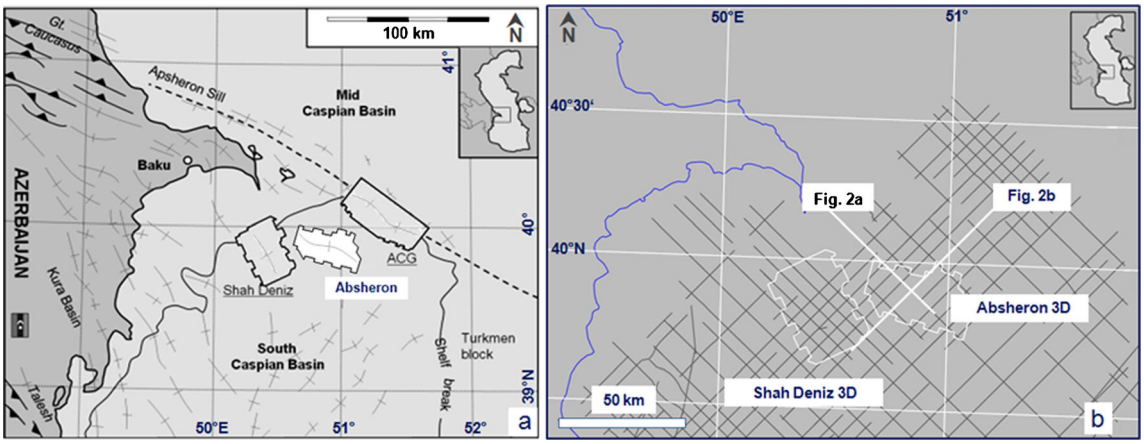

Fig. 1 **a** Location of study area in the South Caspian Basin (modified from Richardson et al. 2011; *ACG* Azeri-Chirag-Guneshli 3-D survey). **b** Seismic datasets comprising two 3-D grids (*encircled in white*) and a larger, regional 2-D grid. *White lines* Seismic profiles of Fig. 2a, b

(2011). In the present article, the four MTDs are numbered MTD 1 to MTD 4 from the top of the section downward.

Figure 2b gives a good synthetic view of MTD 2 from the upslope scar down to the frontal splay. It shows the tripartite subdivision of the MTD into a proximal extensional zone, a central translated raft extending some 10–12 km along the trend of the profile (about 45° with respect to the direction of the glide), and a distal complex zone that appears heavily faulted and buttressed against a frontal ramp; finally, there is an emergent unit that tapers out distally. As can be seen from the proposed reconstruction of the pre-failure geometry (dotted white line), sediment previously covering the area of interest prior to slope failure was evidently remobilized into MTD 2 (dashed white line).

Figure 2c is a TWT map of the seafloor based on the Absheron 3-D seismic survey, showing the Absheron mud volcano (MV) surrounded by an irregular seafloor. The rugged morphology reflects the complexity of the underlying MTD 2, whereas the smoother topography in the northern part reflects the burial of MTD 2 by more recent sediments.

Data sources

Seismic data

Three seismic datasets were available for this study (see grid locations in Fig. 1b). These comprise a regional 2-D seismic grid oriented NW–SE and NE–SW with a spacing of ca. 5 km, and the Shah Deniz 3-D survey available for correlation purposes (cf. above).

The Absheron 3-D seismic survey was shot in 1997 over the Absheron anticline, with both pre-stack time migration (PSTM) and pre-stack depth migration (PSDM) processing available. This survey is proprietary to the companies that operate the Absheron Block. Spectral analysis of the study interval indicates that the observed spectrum is best fitted by a 30–35 Hz Ricker wavelet (Hosken 1988) depending on the profiles, giving an average resolution of 12 m with a velocity of 2,000 m s^{-1}. The limit of visibility (see Brown 2011a, 2011b) is much higher due to the high signal-to-noise ratio in the shallow subseafloor section studied here.

This 3-D survey acquired in 1997 has been reprocessed several times since then. The most recent PSTM processing (version of 2011) was used in the present article. A coherency cube was derived from the amplitude cube for the analysis of deformations and faults. On the amplitude cube, a downward increase of acoustic impedance corresponds to a positive amplitude (peak). In the figures, these data are represented by a grey-shade scale, the darker tones denoting positive amplitudes. Scales on seismic profiles are in seconds (s) two-way travel time (TWT).

Well data

Information from one well was available for the study area. Well calibration for the upper ca. 500 m of the sediment pile is based on a selected set of logs acquired while drilling, comprising gamma-ray, deep- and medium-resistivity, and sonic logs. Ditch cuttings were not recovered in the early phases of drilling. The only available geological information is therefore an approximation of the lithology, i.e., sand vs. shale, within the local context of the Quaternary of the Caspian Sea.

In addition, the sonic log data served to roughly convert TWT thickness into actual thickness. The sonic readings range from 140 to 160 μs/foot, which corresponds to an average velocity very close to 2,000 m s^{-1} over the interval of interest, i.e., 1 ms TWT is equivalent to 1 m.

Results

The seismic data reveal evidence of a large crater-like feature. In Fig. 3a and b, the cross-sectional views show a conspicuous

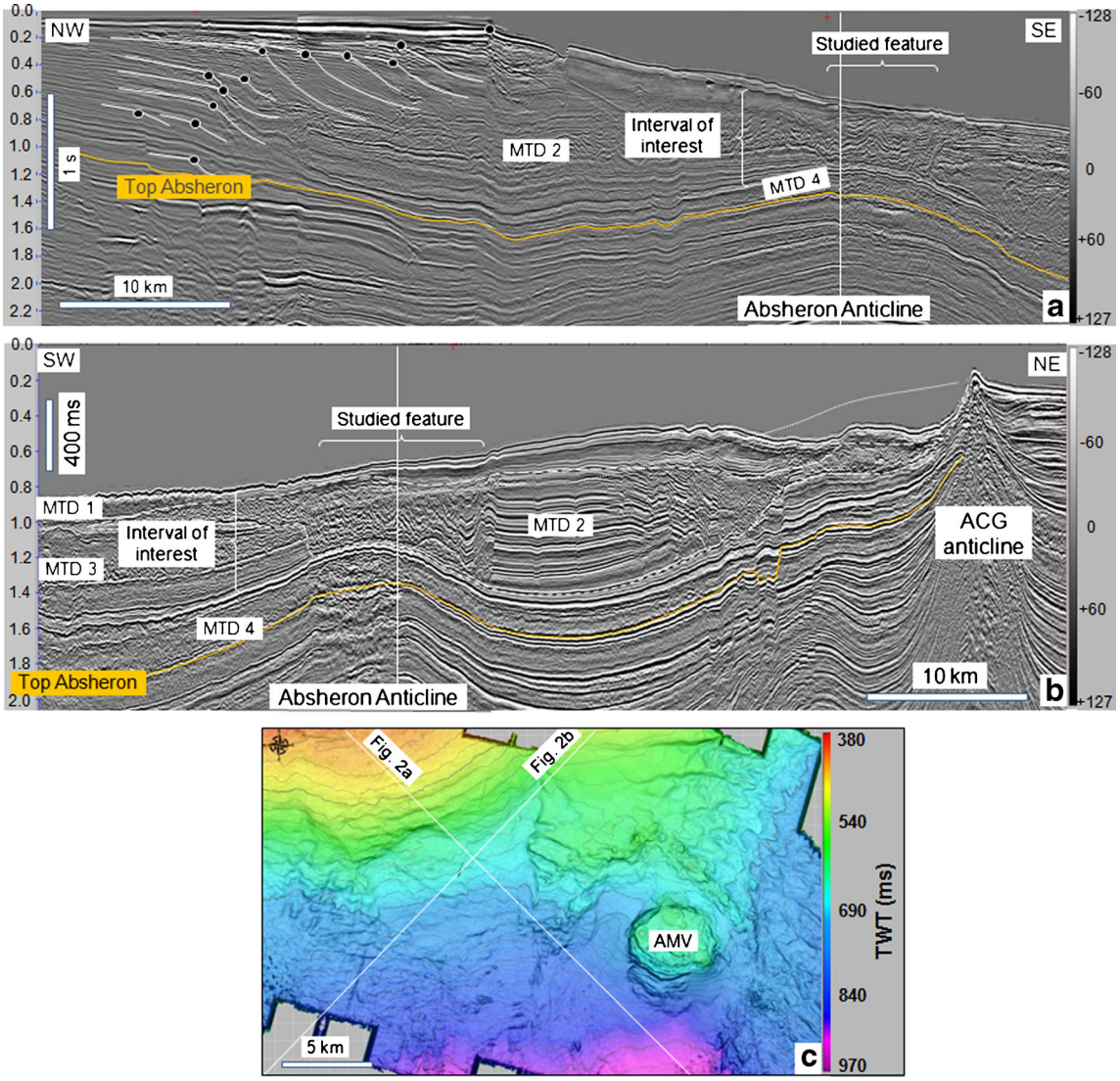

Fig. 2 **a** Seismic stratigraphy of the interval of interest above the top Absheron marker: *MTD 1 to 4* main mass-transport deposits. *Vertical white line* Intersection with profile in **b**, near the crest of the Absheron anticline. **b** Tripartite architecture of MTD 2 with a reconstruction of the situation prior to gliding. *Dashed white line at bottom* Base of MTD 2, *long white dashes* top of remobilized interval, *dotted white line* interpreted morphology of the slope prior to failure, *vertical white line* intersection with profile in **a**, *ACG* Azeri-Chirag-Guneshli anticline, within which a complex of three oil fields is located. **c** TWT (ms) seafloor map based on the Absheron 3-D survey. *AMV* Absheron mud volcano. Note that the actual profiles extend far beyond the limits of the sections in panels **a** and **b** (cf. Fig. 1b). Grey scales in **a** and **b** represent normalized acoustic amplitude

truncation surface (purple horizon) where about 200 ms of the adjacent sedimentary succession are missing in the central part of each cross-section. The purple horizon coincides with the basal detachment surface of MTD 2. The flat bottom is reminiscent of the basal shear surface ramps described by Bull et al. (2009, their Fig. 7) in the headwall domain of large MTDs.

Figure 3c is a TWT thickness map of the interval between the brown horizon just below the crater and the basal detachment surface of MTD 2 (purple horizon). This map view indicates that the crater is a subcircular, closed domain that covers about 50 km^2 with a diameter of ca. 8 km. This contrasts with classical ramps of the basal shear surfaces of MTDs, which commonly open downslope in map view.

Seismic stratigraphy

Mass-transport deposits 2, 3, and 4 occur in large parts of the Absheron 3-D survey and extend beyond its limits. MTD 2 fills the crater and covers the whole survey, with the exception of the Absheron mud volcano. MTD 3 is restricted to the southern flank of the Absheron anticline, and is truncated by the southern edge of the crater. MTD 4 is conspicuous enough to make a convenient stratigraphic marker, but is not directly related to the crater.

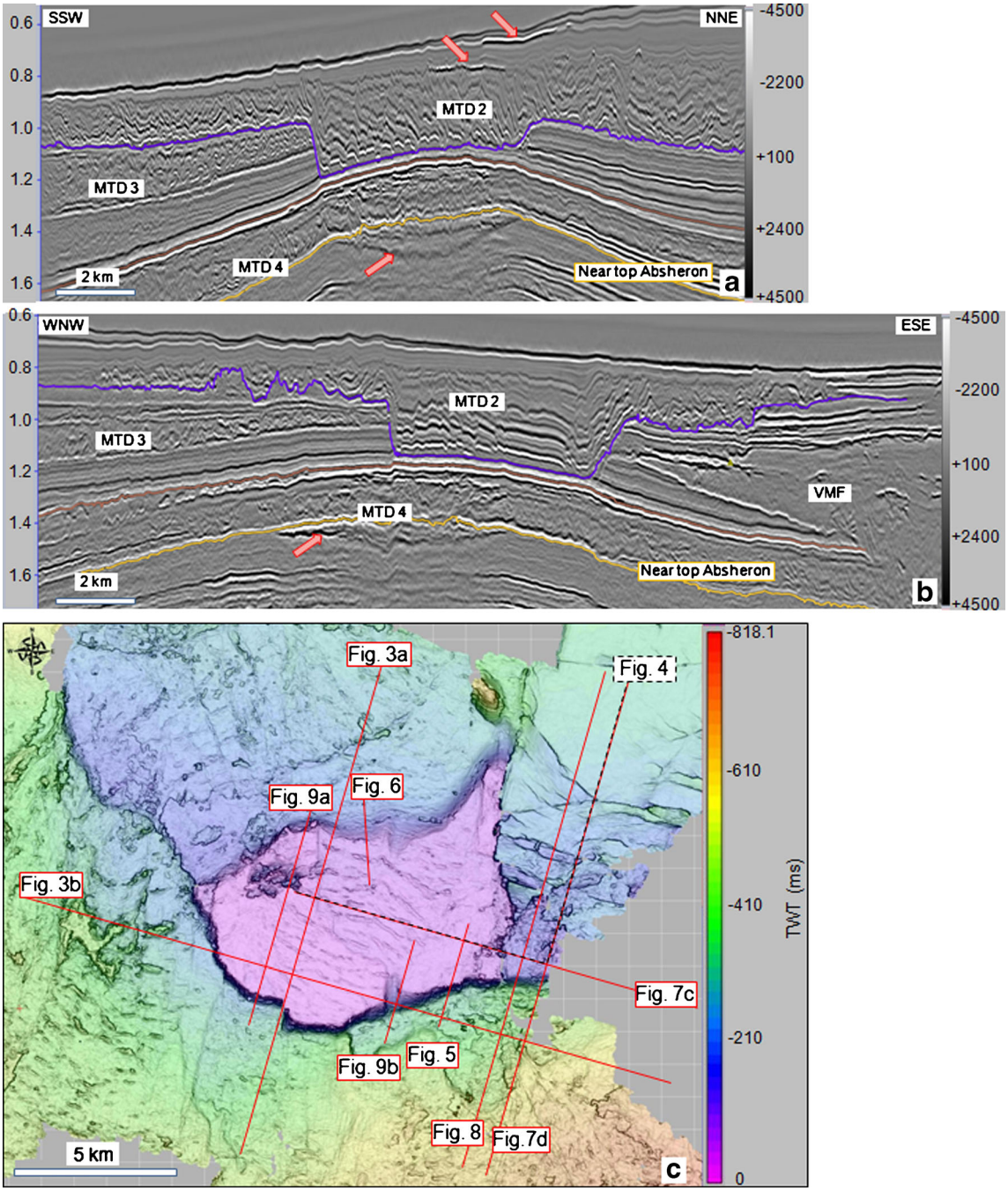

Fig. 3 Seismic profiles across the crater at the crest of the anticline. **a** Dip cross-section highlighting important horizons: *brown line* highest continuous horizon unaffected by sediment removal, *purple line* basal detachment surface of MTD 2. *Red arrows* Seismic indicators of shallow gas pockets. **b** Strike cross-section. *VMF* Volcanic mud flows from the Absheron MV. **c** TWT (ms) thickness map between the purple and brown horizons shown in **a** and **b**, with dip overlain in semi-transparency for relief rendering. Grey scales in **a** and **b** represent seismic amplitude

Some layers are undisturbed in certain parts of the study area, but are remobilized by mass transport in others. The same layer can reappear above a deeper in situ occurrence, being duplicated by the emergent front of one of the MTDs, or come to lie one above the other due to remobilization by a previously emplaced MTD.

The seismic stratigraphy of the interval of interest was established in the NE part of the study area where the initial succession was least disturbed by slope failure. Figure 4 reports an arbitrary seismic profile extending from this well-preserved zone (cf. whole stratigraphic succession) into the crater, where it crosses the trajectory of exploration well #1. Eight horizons numbered H1 to H8 were identified and correlated over as much of the area as possible, from the undisturbed zone into the MTDs. The crater corresponds to the local disappearance of most of the interval comprised between horizons H2 and H4;

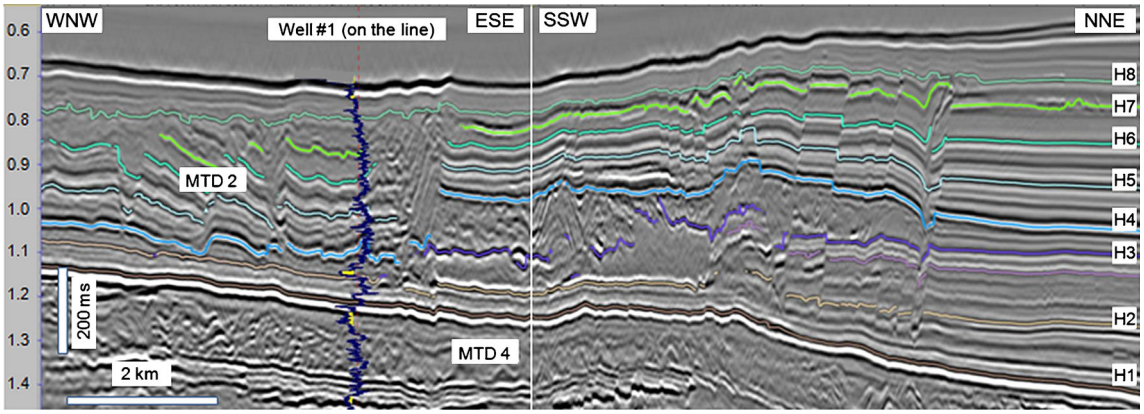

Fig. 4 Definition of seismic horizons and calibration of the lithology at well #1. The vertical profile shown at the well location is a gamma-ray log, with low radioactivity intervals (interpreted as sands) highlighted in *yellow*. The sand interval below the cyan H4 marker in the well corresponds to the Q sands. Vertical scale represents TWT (s)

both these horizons can be distinguished throughout the study area, whereas H3 is absent inside the crater (Fig. 4).

Based on lithological control provided by the gamma-ray log of well #1 (cf. Fig. 4), the only interval that appears to depart from the mud baseline (trend of high-radioactivity intervals) is a ca. 20-m-thick sediment body with low radioactivity near the H2 reflector, likely to correspond to a sand-bearing interval in the present context. This is interpreted as belonging to the regional Q sands Formation.

Morphology and architecture

One way of visualizing the depositional morphology of an irregular sedimentary surface (e.g. an erosion surface) deformed by post-depositional structuring (e.g. folding) is to calculate the isopach between this irregular surface and a paleohorizontal surface above or below (Andresen 1962). The paleohorizontal surface and the irregular surface must have been deformed simultaneously. This approach was applied here to visualize the pre-folding geometry of the basal detachment of MTD 2, by computing the TWT thickness map between the basal detachment surface and the underlying horizon H1, the latter not affected by mass failure. The resulting map is shown on Fig. 3c. It depicts an overall upward shoaling toward the south, with the notable exception of the crater, where there is a drop of about 200 ms. In addition, the dip in overlay indicates three contrasting types of lateral contact between the crater and the surrounding intervals: the southern edge is characterized by high dips (ca. 30° on a 200- to 400-m-wide strip), whereas the northern edge has much gentler inclinations of about 15°; the eastern edge is characterized by a very short and abrupt contact.

Southern edge

The southern part of the crater is bounded by a steep edge showing truncation of the internal reflections of the interval comprised between H1 and H3, and of the overlying MTD 3 (Fig. 3a). Using 2,000 m s^{-1} as interval velocity, the dip of the ramp is about 35° (Fig. 5). The seismic profile also shows a large-scale raft more than 1 km long conformably resting on the truncation surface.

Northern edge

Most of the northern edge shows a very different geometry, with the internal reflections of the interval between H2 and H3 wedging toward horizon H2, accompanied by thinning for the upper layers and gliding at the base. The top of the interval, just below the detachment surface of MTD 2, appears to downlap onto the lower strata of the package (Fig. 6). The angle of apparent downlap is about 10°.

Eastern edge

The eastern edge of the crater is the most complex. Here, the set of blocks and rafts of MTD 2 is separated from the underlying continuous-parallel interval by a ca. 200-ms-thick transparent to chaotic seismic package (Fig. 7). The TWT maps of horizon H4 (lowermost recognizable horizon within MTD 2) in Fig. 7a and of the basal detachment surface of MTD 2 in Fig. 7b, as well as the seismic profile in Fig. 7c show that the basal detachment surface in the eastern block lies at the same level as in the adjoining crater. H4 (where it could be identified) lies just above the detachment surface in the crater, and some 200 ms TWT above it in the eastern block.

The WNW–ESE seismic cross-section in Fig. 7c also reveals that the interval between the detachment surface and H4 in the eastern part of the profile is highly irregular, affected by thrusts rooting in the Absheron MV complex (highlighted in orange). High-amplitude markers develop in the volcanic mudflows (Fig. 7d), both in the autochthonous southern part of the profile

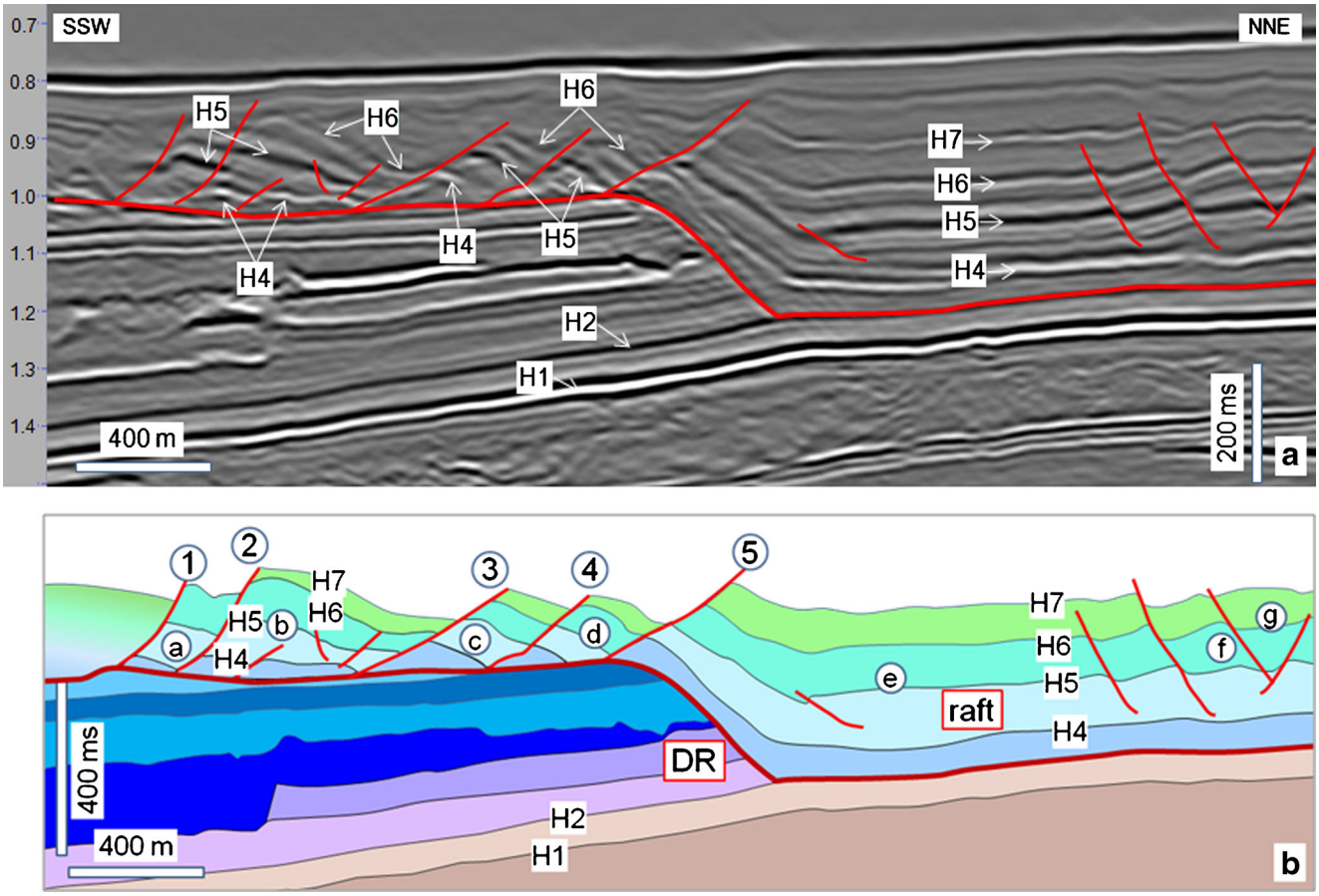

Fig. 5 Seismic profile showing the general stratigraphic architecture with the truncation of underlying horizons at the southern edge of the crater. *DR* Distal ramp of MTD 2. Vertical scale represents TWT (s). Note that individual horizons could not be identified in the southernmost part, possibly due to massive faulting below seismic resolution

and in the deformed part above. In map view, these high-amplitude markers show grooves radiating from the Absheron MV. Combined with the presence of thrusts (Fig. 7c), and a general wedging of the chaotic masses away from the volcano, this morphology suggests that the high-amplitude markers separate masses emanating from the volcano.

The N–S seismic cross-section in Fig. 8 reveals that the H3–H4 interval (medium blue in Fig. 8b) thickens and progressively loses its internal stratification from the northern part (cf. the reference area for defining the stratigraphy) to the middle chaotic part. The overlying series (H4–H7) are faulted, but retain their internal character throughout. Some of the faults are restricted to this upper interval, whereas others cross the whole interval down to H2. Basically, the data for this eastern block are very similar to those for the southern edge of the crater, but with the interposition of a 200-ms-thick chaotic interval between the basal detachment surface of MTD 2 and the series of tilted blocks and rafts above. In other words, removing the middle chaotic mass (cf. white outline in Fig. 7d) from the eastern block would make it similar to the crater.

MTD 2 basal layer

In the study area, mass-transport deposit 2 essentially consists of a series of individual blocks with well-preserved stratification separated by normal faults, commonly with domino-style morphology. In most cases, seismic reflections within blocks are parallel, with limited (if any) internal wedging restricted to the very top. Overall, the deformation of the blocks above the detachment surface is accommodated by the basal layer below H4 (Figs. 4 and 6). In addition to this deformation at the scale of the individual block, several areas show irregular masses with transparent seismic facies interposed between the basal detachment surface of MTD 2 and the layered tilted blocks that make it. Two such patches occur inside the crater (Fig. 9). These are local and relatively small; similar transparent/chaotic bodies can be found outside the crater, always on a scale similar to that of Fig. 9a.

MTD 2 distal ramp

A systematic change occurs across the distal ramp of the crater, from well-organized blocks limited by normal faults

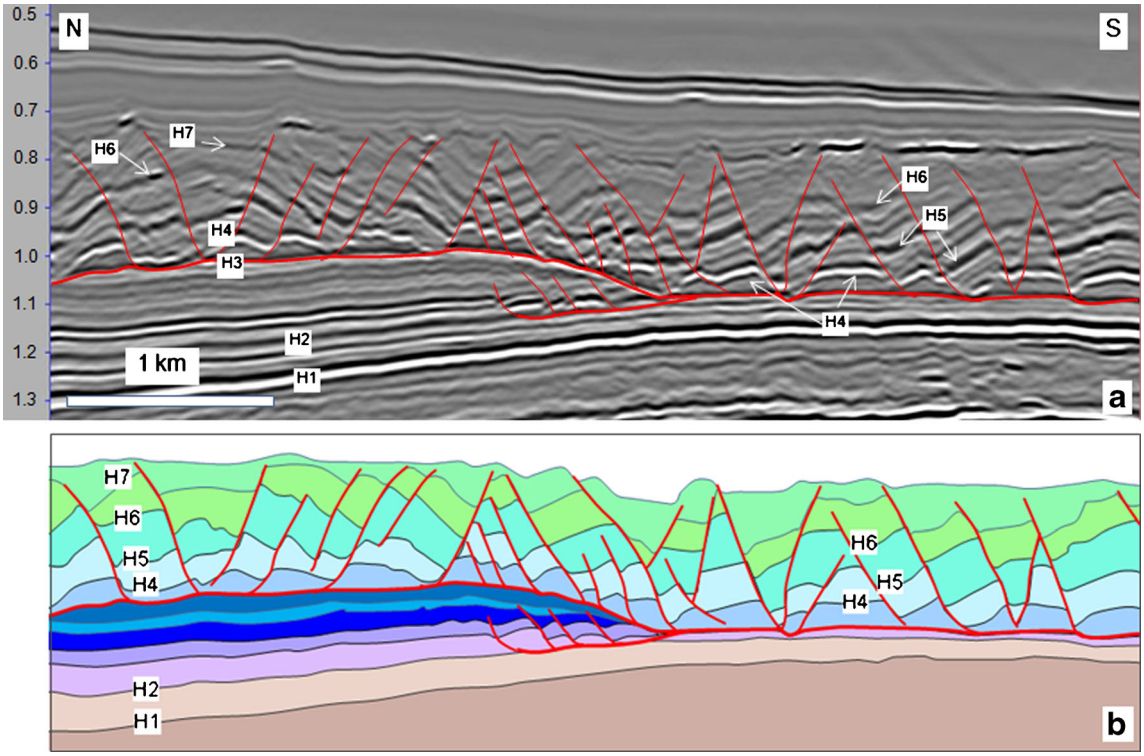

Fig. 6 Seismic profile showing the stratigraphic architecture of the northern edge of the crater, with evidence of wedging and thinning of the H2–H3 interval down onto the H2 horizon. Vertical scale represents TWT (s)

to poorly defined tilted blocks limited by normal, but much flatter faults (Fig. 5). Upslope of the frontal ramp, the dip of the faults is about 50°, whereas downslope it ranges from 25° to 35° only. In Fig. 10a–d, a series of sketches interpreting the emplacement of MTD 2 along the cross-section of Fig. 5a shows how gliding on a sole of plastic material could transform a large continuous raft into a series of extended blocks with low-angle normal faults. The same evolution above the distal ramp can be observed in Fig. 8.

Shallow gas

Seismic anomalies considered as indicative of shallow gas are well developed around the crest of the Absheron anticline. The most prominent occur within the crest of the anticline just below the top Absheron marker (Fig. 3a, b). The profile in Fig. 3a shows an exact coincidence between the crater and the underlying shallow gas accumulation, whereas the two features are offset in Fig. 3b. The strong negative amplitude observed just above the "near top Absheron" horizon is interpreted to reflect the decrease of impedance associated with the presence of gas. The strata-secant irregular horizon below is interpreted as the gas–water contact of this shallow accumulation, structurally horizontal but pushed down by the decrease of seismic velocities caused by gas.

Bright negative amplitude patches are observed just below the seafloor in Fig. 3a. Such anomalies are classically interpreted as evidence of shallow gas (Brown 2011a).

Discussion

The study area lay in deep water throughout deposition of the interval of interest (Fig. 2a). Well #1 (Fig. 4) shows that sedimentation was dominated by shale during that time, with the exception of the 20-m-thick Q sands deposited around the time of marker H3. The deposits of the interval of interest are thus interpreted as dominant hemipelagic mud sometimes reworked by en masse resedimentation (MTD 2 and MTD 3). The only 20-m-thick sandy interval (Q sands) represents a turbidite lobe complex in the deep-water context.

The crater is defined by the local absence of the H2–H3 interval, along with the abrupt disappearance of MTD 3 along its southern edge. Most of the circumference of the crater is characterized by truncations of the H2–H3 interval below the base of MTD 2.

The fact that MTD 3 was also removed during the process means that truncation postdates the emplacement of MTD 3, itself postdating deposition of the last deformed interval: sediment removal therefore took place after deposition of horizon H5. At the same time, MTD 2 that now fills the crater was emplaced around the time when H8 was deposited, with possible early movements in the H7–H8 interval (wedges observed locally). In addition, the wedging of the H2–H3 interval observed along the northern edge of the crater (Fig. 6) is difficult to explain as a depositional feature in the deep-water context, and is not compatible with seafloor erosion either. It appears therefore that the crater formed as a

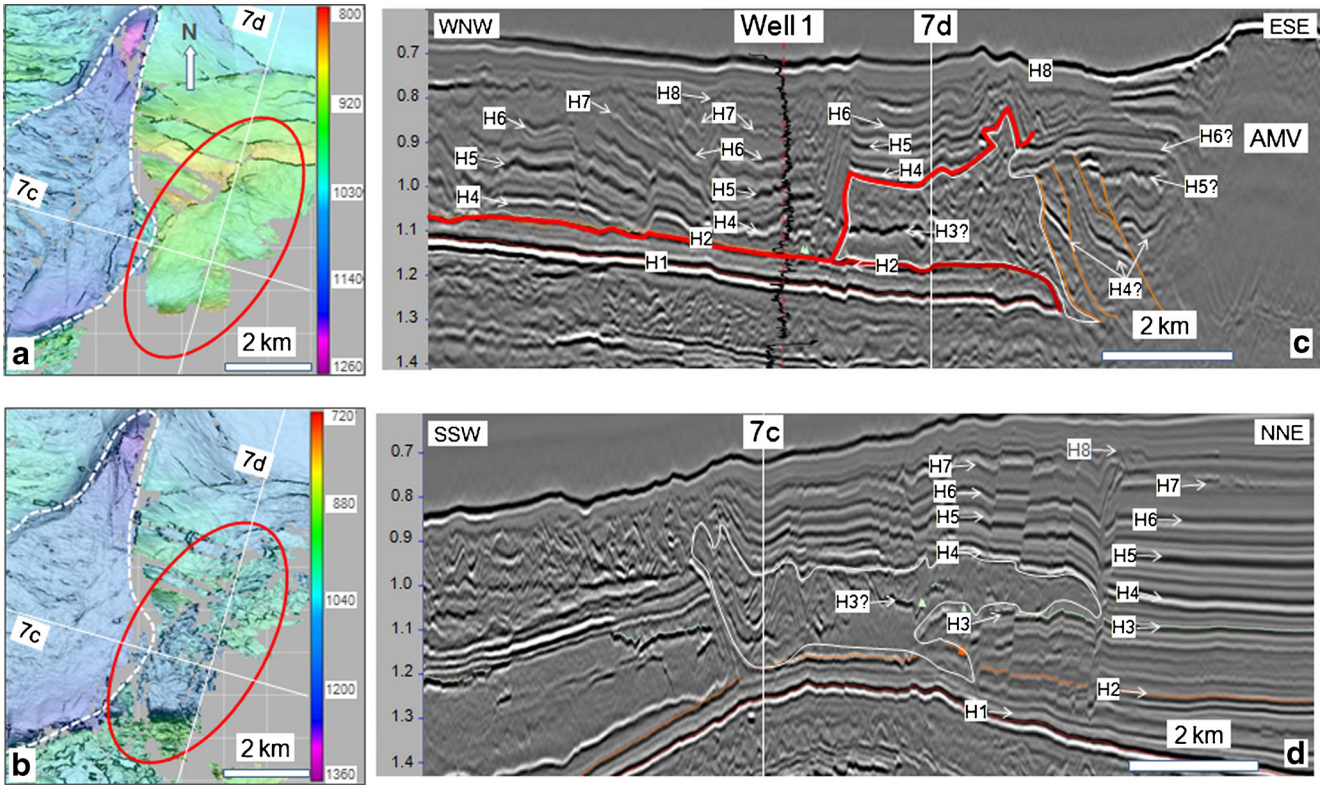

Fig. 7 Eastern edge of the crater. **a** TWT map of the H4 horizon, which lies about 300 ms higher in the eastern block (*red ellipse*) than in the crater. **b** TWT (ms) map of the basal detachment horizon, which lies at approx. the same level in the block as in the crater. **c**, **d** Outline (*white*) of the chaotic or transparent mass interpreted as representing material from an intermediate stage of crater evacuation, causing local expansion of the interval between the detachment surface and the H4 horizon. In **c**: *vivid red contour* basal detachment surface of MTD 2, *red line* base of chaotic mass, *orange lines* interpreted thrusts, *AMV* Absheron mud volcano. In **c** and **d**: *white vertical lines* intersection of the two profiles; vertical scales represent TWT (s)

subsurface evacuation feature, from which at least 6 km^3 of hemipelagites and a wedge of MTD 3 representing about half this volume were removed after burial. Several scenarios are examined below to account for this removal of about 10 km^3 of mud under cover.

Evacuation upward through cover

Evacuation upward through sedimentary cover has been explored in numerous publications this last decade. Notably, Riis et al. (2005) documented giant evacuation craters along the Norwegian Atlantic margin. Based on biostratigraphy from a well that penetrated the features, they concluded that several km^3 of sediment had been evacuated upward from those craters, through an MTD while it was gliding downslope. Furthermore, they observed seismic evidence of gas in the immediate vicinity of the craters, and interpreted the presence of gas as a way of increasing the density inversion between the evacuated formation (siliceous ooze) and its overburden. In the case documented by Riis et al. (2005), the evacuated material is readily observable above the MTD that fills the craters. In the case of the crater examined in the present study, there is no such evidence; nevertheless, part of the transparent series that constitute the uppermost part of MTD 2 could have resulted from a similar phenomenon, i.e., have been evacuated up through the MTD while it was being emplaced. Visual volume comparison indicates that the thickness between H7 and H8 is much less on average than the "missing thickness" of the crater, so that only part of the missing series could have been evacuated in this manner (about 10% at most, based on visual estimation).

Other evacuation features have been described by Imbert and Ho (2012) for the Carnarvon Basin, Australia. Those features are conical, with diameters of a few kilometers and typical depths of a few hundred meters. Consistent with the findings of Sultan et al. (2010) on present-day hydrate pockmarks, the conical features were interpreted as collapsed hydrate pockmarks. In that case, no indication of the evacuated material could be found above; Imbert and Ho (2012) proposed that it was evacuated as sediment plumes, and redistributed over wide areas of the Carnarvon slope.

Evacuation by lateral push/shearing

The presence of seismically transparent packages inside (Fig. 9) and around the crater suggests that the material

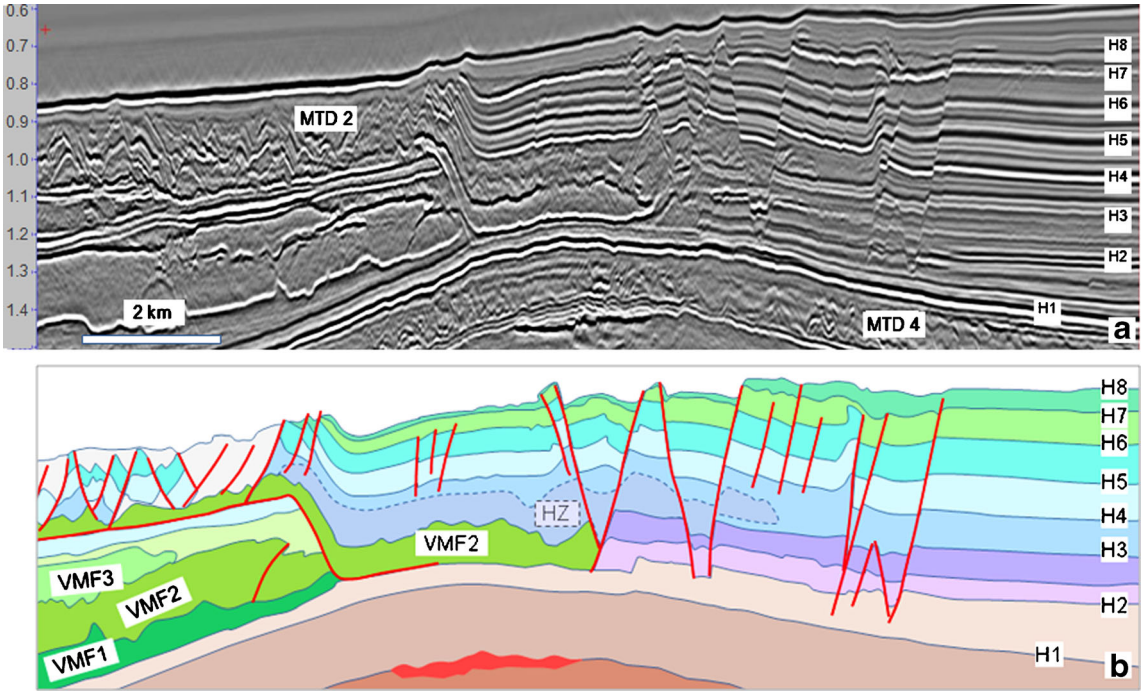

Fig. 8 Seismic profile (**a**; vertical scale represents TWT in s) and interpretation (**b**) of the architecture of the eastern block. The stratal configuration is quite similar to that on Fig. 5 for the southern edge of the crater, but without any loss of material below H4. In **b**: *VMF* Volcanic mud flows from the Absheron MV, *HZ* homogenized zone with a chaotic/transparent package interpreted as representing material of the pre-evacuation stage, *red patch below MTD 4* same shallow gas anomaly as that marked by a red arrow below top Absheron in Fig. 3

initially filling the crater in the H2–H3 interval has been homogenized below seismic resolution and deformed, so that most of it may have been evacuated by lateral shearing (Fig. 5b–d). All these volumes with a transparent character presently lie below H4, commonly between H4 and the MTD 2 basal detachment surface in the crater, or between H4 and H2 (Fig. 7c, d). These are therefore interpreted either as local remnants of the remobilized material, or as deformed sediment that failed to be evacuated.

The character of the eastern block shown in Figs. 7 and 8, where the H3–H4 interval progressively loses its stratification from the north into the crestal area of the Absheron anticline, is interpreted to reflect the fact that the H3–H4 interval is more susceptible to loss of cohesion when deformed than the overlying and underlying series, so that this sole interval was homogenized (at seismic scale at least) in the eastern block while the rest of the succession remained undisturbed for a start. Subsequent gliding transported the whole package along a basal detachment surface close to H2, the distal part becoming frontally emergent (cf. Frey-Martinez et al. 2006). In that respect, the eastern block may represent a failed extension of the crater, thereby preserving an early stage of its formation.

Evacuation toward the Absheron MV

The Absheron MV is located only a few kilometers away (Fig. 2c). It was already active before MTD 2 was emplaced, as shown on Fig. 3b, and still was in a very recent past as indicated by its fresh-looking morphology on the seafloor (Fig. 2c). Thus, material expelled by the mud volcano may have captured material evacuated from the crater. However, the seafloor map (Fig. 2c) shows that the mud volcano stands higher than the crater and, moreover, there is no evidence for the existence of an evacuation canal heading from the crater toward the mud volcano. Such a scenario is therefore considered unlikely at this stage.

Role of gas

The last decade has seen a marked increase in publications evoking the role of gas in triggering submarine landslides in various settings worldwide (e.g., Best et al. 2003; Bünz et al. 2005; Shaw et al. 2012), accompanied by recent confirmatory evidence in, for example, the western Mediterranean (Berndt et al. 2012, Ana submarine landslide complex) and along the Norwegian continental margin (Hill et al. 2012, Storegga slide complex). Sultan et al. (2012) carried out experiments on natural mudstone samples filled by gas-saturated water under confining pressure, recovered by coring from the continental slope of the Gulf of Guinea at about 20 m below seafloor. The experiment showed that lowering the confining pressure resulted in immediate decrease of P- and S-wave velocities. The former indicates that free

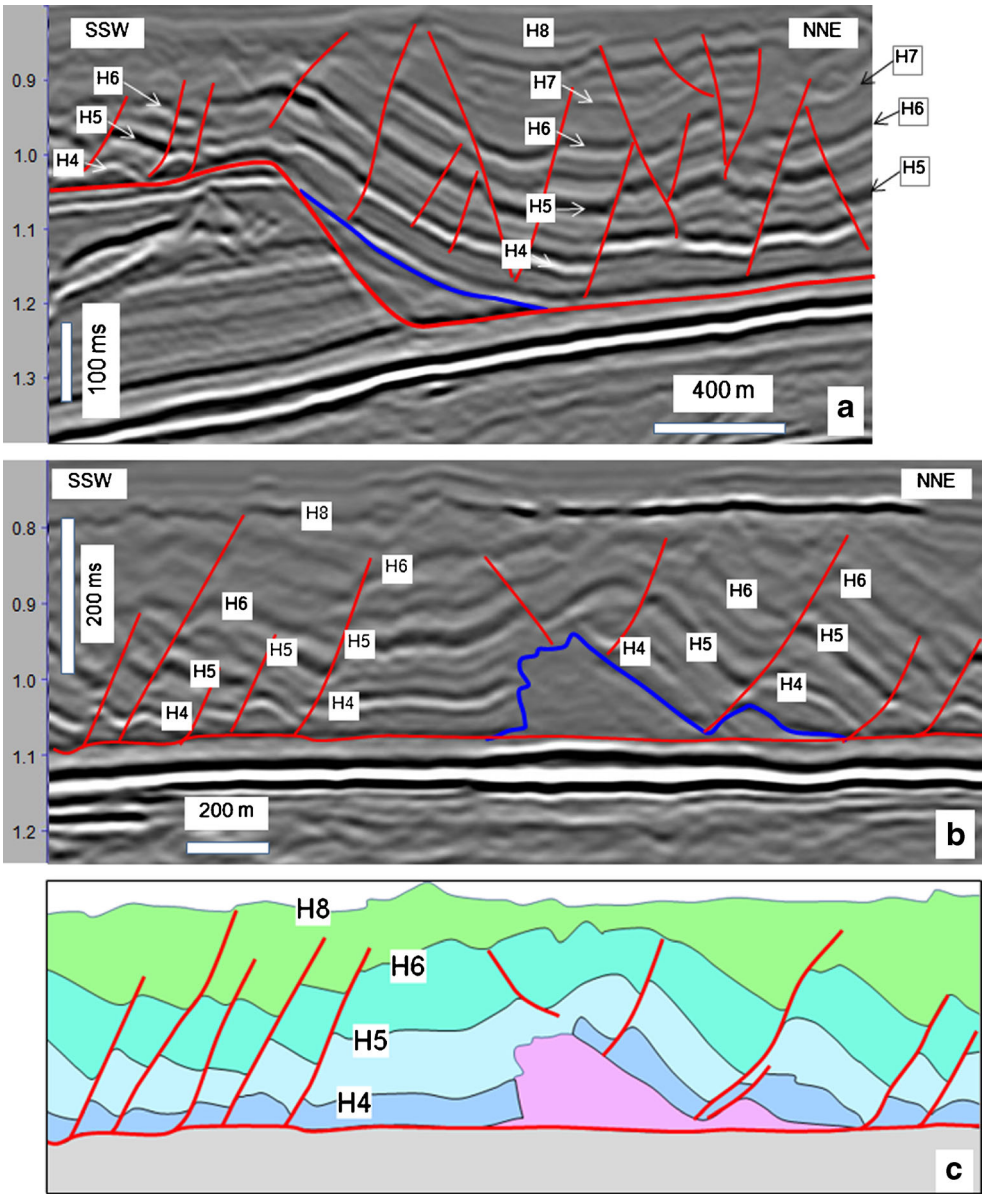

Fig. 9 Residual pods of transparent material occurring between the basal detachment surface of the crater and H4. **a** Transparent body wedged between the truncation surface (*red*) and the base of the rafts of MTD 2 (*blue*) at the southern edge of the crater. **b**, **c** Transparent diapir-like body located in the middle of the crater. *Blue line* Upper envelope of the transparent facies, resting on the detachment surface (*red line*). Vertical scales in **a** and **b** represent TWT (s)

gas was generated in the sample (exsolution), the latter that the actual texture of the sample is damaged, so as to affect the propagation of shear waves (which are insensitive to changes in pore-filling fluid).

Examination of the eastern edge of the crater has shown that the H2–H4 interval is prone to structural damage and homogenization at seismic scale (Figs. 7 and 8). The evacuation crater developed at the crest of the anticline, close to its present-day position characterized by the presence of shallow gas. Combining all these data, gas is interpreted to have played a major role in reducing the resistance to shear of the already weak sediments in the H2–H4 interval above a shallow gas accumulation, probably located in the Q sands reservoir.

Overall, MTD 2 (like all MTDs) became detached along a weak layer in the sedimentary succession. What the crater demonstrates is that this weakness zone was laterally variable and, moreover, that it was thick enough in a particular area to be totally evacuated. The coincidence between the evacuation area and an underlying gas accumulation suggests that gas probably played a significant role in weakening the evacuated layer.

The hydrate issue

Hydrate dissociation has long been suspected to be a possible cause of slope failure (e.g., Sultan et al. 2004; Brown et al. 2006). Gas hydrates have been sampled at the seafloor in the South Caspian Basin at water depths (475 and 660 m; Ginsburg and Soloviev 1994) similar to those of the present study. Moreover, Diaconescu et al. (2001) and Knapp and Knapp (2004) reported 2-D seismic indications of a possible

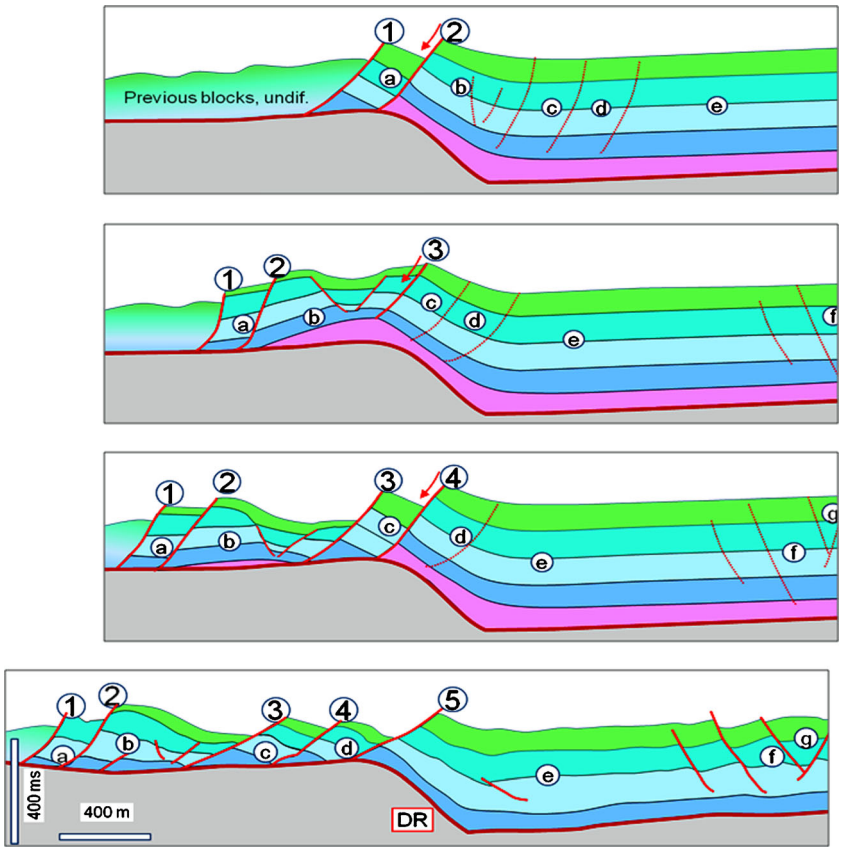

Fig. 10 Interpreted evolution of MTD 2 entailing progressive disorganization as it flowed across the distal ramp (*DR*) of the crater. The undifferentiated material (*previous blocks, undif.*) evacuated at an earlier stage should consist of the same material, and was probably deformed in a similar way, as the differentiated material that followed (cf. main text for details)

bottom-simulating reflector (BSR). The available 3-D dataset however indicates that this BSR-like horizon is highly irregular and coincides with the base of one of the main mudflows emanating from the Absheron mud volcano. Although the possibility of there being hydrates in the study area cannot be discounted, thorough evaluation of the available 3-D seismic data did not reveal any evidence concomitant with a bottom-simulating reflector. The abundant bright patches interpreted as shallow gas suggest that methane is present in a gaseous state rather than in the form of hydrates, at least under present-day conditions.

Conceptual model of crater evacuation

Based on the interpretations presented above, a four-stage conceptual model of crater evacuation is proposed. Figure 11a depicts the initial situation before the onset of failure of MTD 2. MTD 3 was already in place at that time, sealed by H6. The thin yellow layer represents the regionally known Q sands, a remnant of which is observed in well #1 (Fig. 4).

Stage 1

Stage 1 entails saturation with gas above a shallow reservoir (Fig. 11b). Gas actively migrating from the deep progressively filled the Q sands reservoir. As soon as free gas started accumulating at the crest of the anticline, it began diffusing into the overburden. As the accumulation filled up, the zone of gas diffusion increased, and so did the gas concentration above the accumulation.

Stage 2

Stage 2 entails inception of gliding (Fig. 11c). MTD 2 covers a much wider area than the crater. The triggering factor therefore is interpreted to be the general failure of the slope along the main weakness level(s) of the sedimentary succession, close to H3. As shown by the pervasive normal faulting that affects MTD 2, its emplacement corresponds to an extension, therefore to thinning. As a result, the lithostatic pressure exerted by the overburden of the Q sands decreased when this overburden was thinned by mass failure. A relative sea-level fall might have been the triggering factor, but this is hypothetical and not essential to the reasoning.

Stage 3

Stage 3 entails thinning and degassing (Fig. 11d). The drop in lithostatic pressure resulted in gas exsolution from the crater area. The resistance to shear of this gas-saturated unit then became less than that of the main detachment level. As a

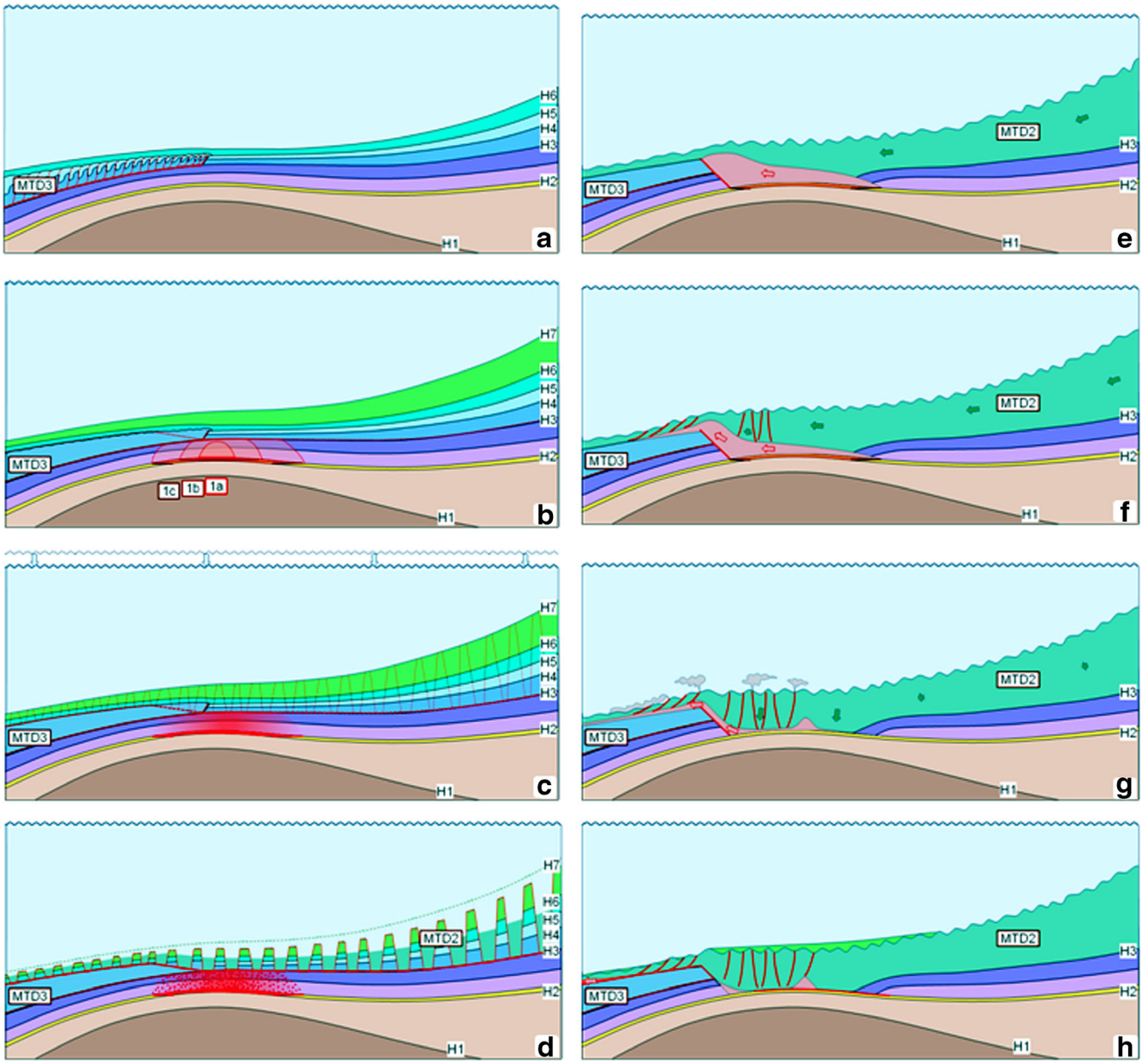

Fig. 11 Conceptual model of crater development. **a** Stratigraphic situation prior to emplacement of MTD 3. **b** Progressive infiltration of the Q sands (*yellow*) by gas (*red overlays 1a–1c*); the semi-transparent pink zones above the gas pockets indicate impregnation of the overburden. **c**, **d** Before/after comparison of MTD 2 emplacement; the dotted line in **d** marks the top of the failed mass before gliding; red dots in the gas-impregnated interval symbolize free gas bubbles produced by exsolution. **e** Gliding of MTD 2 (*green*, individual blocks not shown). **f** Weakening and homogenization of the gas-impregnated zone, which becomes prone to plastic deformation and evacuation by shear at the base of the still flowing MTD 2. **g** Minor contributions from suspended mud plumes ("clouds") emanating from faults. **h** Final stage after MTD 2 stopped moving, but prior to subsequent burial by more recent sediment. *Surficial thin green layer* Sediment deposited by mud plumes (see **g**)

result, shearing that regionally occurred at the level of H3 was transferred down into the H2–H3 interval, which subsequently behaved as a plastic mass. From this point on, deformation of the plastic H2–H3 interval accommodated the differences in overload by deflating where the overburden was higher, and inflating where it was lower. On the contrary, the eastern block that lay laterally to the gas accumulation was deformed and inflated, but did not fail completely as happened in the crater itself.

Stage 4

Stage 4 entails gliding on the weakened (plastic) seal of the Q sands (Fig. 11e–h). The progressive movement of MTD 2 displaced and pushed the plastic crater fill along the basal detachment surface and over the edge of the crater, thereby flattening its top above the crater. Along the northern edge of the crater, the back wedge of the gas-impregnated sediment was squeezed out to the south, resulting in local

subsidence of the northern side of the crater and eventually producing the wedging and apparent downlap observed on the profile in Fig. 6. Under the pressure of the upslope MTD 2, its frontal part formed a bulge against the distal buttress composed of non-impregnated H2–H3 sediment beyond the shallow gas accumulation in the Q sands. The soft material was evacuated along the base of the frontally emergent part of MTD 2, with a possible contribution of upward plume leakage through the MTD 2 sediment.

Once most of the homogenized and softened material was evacuated, a thick pile of sediment abutted against the non-gassy H2–H3 deposits and the overlying MTD 3. The resulting blockage caused a few minor remnants of the homogenized mass to be left behind in the crater in the form of a downslope wedge and a few "diapir-like" structures close to its apex.

Conclusions

The study of this evacuation feature is interpreted to illustrate the complex interplay between slope failure and a preexisting shallow gas accumulation, in this specific case with a positive feedback. In a more general context, this type of sediment–gas interaction may explain ramp-and-flat geometries at the base of mass-transport deposits, when the basal detachment surface comes down above a structural high at the time of MTD emplacement. This interpretation can probably be considered highly likely when stepping down occurs over a closed area in map view. A published example of such a behavior, in which fluid flow is considered as a likely mechanism by the authors, is the set of giant craters observed by Riis et al. (2005) and Lawrence and Cartwright (2010) in the Møre Basin, mid-Norway margin. By contrast, ramp-and-flat geometries such as those shown by Bull et al. (2009) appear to trend downslope, without a clear relationship to a potential hydrocarbon trap deeper down. In such cases, an interpretation based on lithological contrast could be considered more likely than one invoking gas migration from the deep (e.g., Hogan et al. 2013, Hinlopen Slide, Arctic Ocean; Laberg et al. 2014, Jan Mayen Ridge, Norwegian–Greenland Sea).

Moreover, this study demonstrates that the presence of a gas accumulation in the shallow subsurface can significantly modify sediment mechanical properties in its vicinity. The combination of preexisting gas saturation and rapid pressure decrease could explain, for instance, some aspects of mud volcanism and mud diapirism, keeping in mind the warnings expressed by recent papers about the overuse of the latter concept (Day-Stirrat et al. 2010; Morley et al. 2011).

Going further in our general understanding requires a physical approach dealing with the various phenomena involved, in particular an improved knowledge of the balance between gas exsolution by pressure decrease and evacuation of excess pressure through the porous network. The "geologically instantaneous" character usually interpreted for mass failure (see, for instance, the Storegga slide and associated tsunami; e.g., Bondevik et al. 2005) ensures that rapid unloading will result in gas exsolution at a faster rate than mud permeability can expel any additional fluid. On the contrary, the result of a eustatic sea-level change or of a tectonic pulse is difficult to assess without taking into account the rates at which each process acts.

Acknowledgements This paper could not have been put together without the discussions the authors have had with a number of colleagues and friends, including Frank Adler, Jan Baur, Martine Bez, Eric Cauquil, Bertrand Chevallier, Jean-Louis Lesueur, Jean-Christophe Navarre, Dan Praeg and Stephan Unterseh. Reviews by Marc De Batist and Christian Berndt greatly helped improving the manuscript. Other useful comments were provided by the guest editor Catherine Pierre and the journal editors. We would like to thank Total and its partners for permission to publish this work. The final interpretation is ours, however, and may not reflect that of Total or its affiliates, especially as regards safety issues.

References

Abdullayev NR (2000) Seismic stratigraphy of the upper Pliocene and Quaternary deposits in the South Caspian Basin. J Petrol Sci Eng 28: 207–226

Ali-Zadeh AA, Aliyeva EG (2004) Stratigraphic architecture of Quaternary succession in the Caspian Basin. In: Ali-Zadeh AA (ed) South Caspian Basin: geology, geophysics, oil and gas content. Nafta Press, Baku, pp 6–18

Allen MB, Jones S, Ismail-Zadeh A, Simmons M, Anderson L (2002) Onset of subduction as the cause of rapid Pliocene-Quaternary subsidence in the South Caspian Basin. Geology 30:775–778

Allen MB, Vincent SJ, Alsop GI, Ismail-Zadeh A, Flecker R (2003) Late Cenozoic deformation in the South Caspian region: effects of a rigid basement block within a collision zone. Tectonophysics 366:223–239

Andresen MJ (1962) Paleodrainage patterns: their mapping from subsurface data, and their paleogeographic value: geological notes. AAPG Bull 46:398–405

Berndt C, Costa S, Canals M, Camerlenghi A, de Mol B, Saunders M (2012) Repeated slope failure linked to fluid migration: the Ana submarine landslide complex, Eivissa Channel, Western Mediterranean Sea. Earth Planet Sci Lett 319/320:65–74

Best AI, Clayton CRI, Longva O, Szuman M (2003) The role of free gas in the activation of submarine slides in Finneidfjord. In: Locat J, Mienert J (eds) Submarine mass movements and their consequences. Kluwer, Dordrecht, pp 491–498

Bondevik S, Løvholtb F, Harbitz C, Mangerud J, Dawson A, Svendsen JI (2005) The Storegga Slide tsunami - comparing field observations with numerical simulations. Mar Petrol Geol 22:195–208

Brown AR (2011a) Chapter 5: Reservoir identification. In: AAPG Memoir 42 and SEG Investigations in Geophysics, no 9. Interpretation of three-dimensional seismic data, 7th edn. Tulsa, Oklahoma, pp 153–197

Brown AR (2011b) Chapter 6: Tuning phenomena. In: AAPG Memoir 42 and SEG Investigations in Geophysics, no 9. Interpretation of three-dimensional seismic data, 7th edn. Tulsa, Oklahoma, pp 199–212

Brown HE, Holbrook WS, Hornbach MJ, Nealon J (2006) Slide structure and role of gas hydrate at the northern boundary of the Storegga Slide, offshore Norway. Mar Geol 229:179–186

Bull S, Cartwright J, Huuse M (2009) A review of kinematic indicators from mass-transport complexes using 3-D seismic data. Mar Petrol Geol 26:1132–1151

Bünz S, Mienert J, Bryn P, Berg K (2005) Fluid flow impact on slope failure from 3D seismic data: a case study in the Storegga Slide. Basin Res 17:109–122

Day-Stirrat RJ, McDonnell A, Wood LJ (2010) Diagenetic and seismic concerns associated with interpretation of deeply buried "mobile shales". In: Wood L (ed) Shale tectonics. AAPG Mem vol 93. Tulsa, Oklahoma, pp 5–27

Deville E (2009) Chapter 5: Mud volcano systems. In: Lewis N, Moretti A (eds) Volcanoes: formation, eruptions and modelling. Nova Science, New York, pp 95–126

Deville E, Guerlais SH, Lallemant S, Schneider F (2010) Fluid dynamics and subsurface sediment mobilization processes: an overview from the Southeast Caribbean. Basin Res 22:361–379

Diaconescu CC, Kieckhefer RM, Knapp JH (2001) Geophysical evidence for gas hydrates in the deep water of the South Caspian Basin, Azerbaijan. Mar Petrol Geol 18:209–221

Evans RJ, Davies RJ, Stewart SA (2006) Internal structure and eruptive history of a kilometre scale mud volcano system, South Caspian Sea. Basin Res 19:153–163

Fowler SR, Mildenhall J, Zalova S, Riley G, Elsley G, Desplanques A, Guliyev F (2000) Mud volcanoes and structural development on Shah Deniz. J Petrol Sci Eng 28:189–206

Frey-Martinez J, Cartwright J, James D (2006) Frontally emergent vs. frontally confined submarine landslides: a 3D seismic characterization. Mar Petrol Geol 23:585–604

Ginsburg GD, Soloviev VA (1994) Mud volcano gas hydrates in the Caspian Sea. Bull Geol Soc Denmark 41:95–100

Hill TM, Paull CK, Critser RB (2012) Glacial and deglacial seafloor methane emissions from pockmarks on the northern flank of the Storegga Slide complex. Geo-Mar Lett 32(1):73–84

Hogan KA, Dowdeswell JA, Mienert J (2013) New insights into slide processes and seafloor geology revealed by side-scan imagery of the massive Hinlopen Slide, Arctic Ocean margin. Geo-Mar Lett 33(5): 325–343

Hosken JW (1988) Ricker wavelets in their various guises. First Break 6(l):24–33

Imbert P, Ho S (2012) Seismic-scale funnel-shaped collapse features from the Paleocene–Eocene of the North West Shelf of Australia. Mar Geol 332(334):198–221

Jackson J, Priestley K, Allen M, Berberian M (2002) Active tectonics of the South Caspian Basin. Geophys J Int 148:214–245

Jones RW, Simmons MD (1996) A review of the stratigraphy of Eastern Paratethys (Oligocene-Holocene). Bull Nat History Mus geol suppl 52:25–49

Kalani M, Khodabakhsh S, Amirbehboudi C (2008) Seismic expression and inferred depositional environments of Plio-Pleistocene sedimentary sequences in the southwestern Caspian Sea. Geo-Mar Lett 28(1):31–41

Knapp CC, Knapp JH (2004) Absheron allochthon of the South Caspian Sea: evidence for slope instability in response to gas hydrate dissociation. In: Ali-Zadeh AA (ed) South Caspian Basin: geology, geophysics, oil and gas content. Nafta Press, Baku, pp 257–268

Kroonenberg SB, Simmons MD, Alekseevski NI, Aliyeva E, Allen MB, Aybulatov DN, Baba-Zadeh A, Badyukova EN, Davies CE, Hinds DJ, Hoogendoorn RM, Huseyenov D, Ibrahimov B, Mamedov P, Overeem I, Rusakov GV, Suleymanova S, Svitoch AA, Vincent SJ (2012) Two deltas, two basins, one river, one sea: the modern Volga Delta as an analogue of the Neogene Productive Series, South Caspian Basin. In: Giosan L, Bhattacharya JP (eds) River deltas - Concepts, models, and examples. SEPM Spec Publ vol 83. Tulsa, Oklahoma, pp 231–256

Laberg JS, Kawamura K, Amundsen H, Baeten N, Forwick M, Rydningen TA, Vorren TO (2014) A submarine landslide complex affecting the Jan Mayen Ridge, Norwegian–Greenland Sea: slide-scar morphology and processes of sediment evacuation. Geo-Mar Lett 34(1):51–58

Lawrence GWM, Cartwright JA (2010) The stratigraphic and geographic distribution of giant craters and remobilised sediment mounds on the mid Norway margin, and their relation to long term fluid flow. Mar Petrol Geol 27:733–747

Morley CK, King R, Hillis R, Tingay M, Backe G (2011) Deepwater fold and thrust belt classification, tectonics, structure and hydrocarbon prospectivity: a review. Earth Sci Rev 104:41–91

Moscardelli L, Wood L, Mann P (2006) Mass-transport complexes and associated processes in the offshore area of Trinidad and Venezuela. AAPG Bull 90:1059–1088

Planke S, Svensen H, Hovland M, Banks DA, Jamtveit B (2003) Mud and fluid migration in active mud volcanoes in Azerbaijan. Geo-Mar Lett 23:258–268

Popov SV, Rögl F, Rozanov AY, Steininger FF, Shcherba IG, Kova M (eds) (2004) Lithological-paleogeographic maps of Paratethys, 10 maps late Eocene to Pliocene. Courier Forschungsinstitut Senckenberg 250:1–46

Richardson SEJ, Davies RJ, Allen MB, Grant SF (2011) Structure and evolution of mass transport deposits in the South Caspian Basin, Azerbaijan. Basin Res 23:702–719

Riis F, Berg K, Cartwright J, Eidvin T, Hansch K (2005) Formation of large, crater-like evacuation structures in ooze sediments in the Norwegian Sea. Possible implications for the development of the Storegga Slide. Mar Petrol Geol 22:257–273

Shaw J, Piper DJW, Skulski T, Lamplugh MJ, Craft A, Roy A (2012) New evidence for widespread mass transport on the Northeast Newfoundland Shelf revealed by Olex single-beam echo sounding. Geo-Mar Lett 32(1):5–15

Stewart SA, Davies RJ (2006) Structure and emplacement of mud volcano systems in the South Caspian Basin. AAPG Bull 90:771–786

Sultan N, Cochonat P, Foucher JP, Mienert J (2004) Effect of gas hydrates melting on seafloor slope stability. Mar Geol 213:379–401

Sultan N, Marsset B, Ker S, Marsset T, Voisset M, Vernant AM, Bayon G, Cauquil E, Adamy J, Colliat JL, Drapeau D (2010) Hydrate dissolution as a potential mechanism for pockmark formation in the Niger delta. J Geophys Res 115, B08101. doi:10.1029/2010JB007453

Sultan N, de Gennaro V, Puech A (2012) Mechanical behaviour of gas-charged marine plastic sediments. Géotechnique 62:751–766

Vail PR, Audemard F, Bowman SA, Eisner PN, Perez-Cruz G (1991) The stratigraphic signatures of tectonics, eustasy and sedimentology - an overview. In: Einsele G, Ricken W, Seilacher A (eds) Cycles and events in stratigraphy. Springer, Berlin, pp 617–659

Weimer P (1989) Sequence stratigraphy of the Mississippi Fan (Plio-Pleistocene), Gulf of Mexico. Geo-Mar Lett 9:185–272

Yusifov M, Rabinowitz PD (2004) Classification of mud volcanoes in the South Caspian Basin, offshore Azerbaijan. Mar Petrol Geol 21:965–975